Adaption of tribological behavior of a-C:H coatings for application in dry deep drawing

Tom Häfner[1, 2], *Benedict* Rothammer[3*], *Jennifer* Tenner[4], *Kim* Krachenfels[4], *Marion* Merklein[4], *Stephan* Tremmel[3], *Michael* Schmidt[1, 2]

[1]Institute of Photonic Technologies, Friedrich-Alexander-Universität Erlangen-Nürnberg (FAU), Konrad-Zuse-Str. 3/5, 91052 Erlangen, Germany
[2]Erlangen Graduate School in Advanced Optical Technologies (SAOT), Friedrich-Alexander-Universität Erlangen-Nürnberg (FAU), Paul-Gordan-Str. 6, 91052 Erlangen, Germany
[3]Institute of Engineering Design, Friedrich-Alexander-Universität Erlangen-Nürnberg (FAU), Martensstr. 9, 91058 Erlangen, Germany
[4]Institute of Manufacturing Technology, Friedrich-Alexander-Universität Erlangen-Nürnberg (FAU), Egerlandstr. 13, 91058 Erlangen, Germany

Abstract. Nowadays the sheet metal forming industry faces challenges regarding efficient usage of resources and sustainability. One strategy to increase the environmental friendliness is to abandon the application of lubricants. The direct contact between tool and workpiece leads to an intensive interaction which increases friction. Especially for deep drawing processes with long sliding distances, this causes distinctive wear. The tool sided application of carbon based coatings is a well-known approach to reduce friction and wear. Former studies have shown a beneficial behavior of hydrogenated amorphous carbon based coatings (a-C:H) to improve the tribological conditions in contact with steel sheets and aluminium alloys under dry conditions. Within this study the coating process and the resulting coating properties will be analyzed. Afterwards mechanical and laser based surface treatment processes prior and after the deposition process will be investigated to reduce the coating roughness. Different roughness values were achieved by varying the surface treatment processes. The laser based finishing enables a reduction of the S_{pk} values by removing single roughness asperities. In order to identify the necessary process parameters for the laser treatment, an analytical model of the material removal was applied. The laser surface treatment achieved similar roughness characteristics compared to mechanical treatment. In this study the tribological behavior of a-C:H coated tools was analyzed under dry conditions within strip drawing tests. The tribological investigations revealed that for dry deep drawing of zinc coated DC04 a broader range of S_{pk} values leads to acceptable tribological conditions whereas for AA5182 a smoother tool surface has to be ensured to prevent adhesion and utilize the full potential of a-C:H coatings.

Keywords: Tribology, Surface Modification, Dry Deep Drawing

1 Introduction

The deep drawing process is characterized by low energy consumption due to short production cycles and high material efficiency. Facing future economic and environmental challenges, such as the scarcity of fossil fuels, further improvements in today's manufacturing processes are essential. One approach to optimizing sustainability and environmental protection is the elimination of lubricants in deep drawing processes. In this way, environmentally harmful substances in the lubricant can be dispensed. Furthermore, the process chain can be shortened by eliminating time-consuming cleaning steps of the workpiece after forming. The lubricant-free contact leads to solid friction between tool and workpiece, which results in a drastic increase in friction and wear. As a result, forming forces increase, tool life is shortened and workpiece quality is reduced [1]. The role of lubricant can be replaced by a promising approach of tool sided coatings. Diamond-like carbon (DLC) coatings in particular showed a high potential for reducing friction under dry conditions in contact with stainless steel [2] and aluminium alloys [3]. Different tribological conditions are desirable for deep drawing in order to locally impede or facilitate the flow of material and to achieve increased wear resistance in critical tool areas. For this purpose, the development of locally adapted tribological conditions is necessary. In prior studies, tetrahedral amorphous carbon (ta-C) coatings showed the most promising results in minimizing friction and wear in contact with the tested sheet materials: DC04, a mild deep drawing steel and the aluminium alloy AA5182 [4]. Furthermore, a-C:H coated tool surfaces contribute to a certain reduction of friction by reducing adhesion in comparison to blank tool surfaces. In general, a-C:H coatings have a higher adhesive strength than ta-C coatings [5]. DLC modifications in different scales are possible to adapt the tribological properties. The friction behavior can be modified by changing the coating's chemical structure

* Corresponding author: rothammer@mfk.fau.de

with regard to its hybridization states or by reducing the roughness asperities. In order to investigate this influence, a laser based smoothing of coated surfaces is analyzed. On a microscopic scale, the roughness of the coating influences the resulting friction and wear [6]. For this reason, the deposited coatings are subsequently treated by means of surface finishing mechanical brushes or finished by laser ablation. In this study, the tribological behavior of surface modified DLC coatings is evaluated by determining the friction coefficient in strip drawing tests and characterization of the surfaces. Two different initial topographies and two different surface finishes will be investigated.

2 Experimental setup and methodology

Within this study the cold working steel 1.2379 (X155CrVMo12) with a hardness of about HRC 60 ± 1 was used as tool steel for discs and friction jaws. The substrate surfaces were polished, representing the surface qualities of conventional deep drawing tools without preferential direction. Subsequently, the polished surfaces were cleaned in an ultrasonic bath with isopropanol and acetone each for 10 min and 2 min, respectively. As sheet materials the deep drawing steel DC04 with a zinc coating and the aluminium alloy AA5182 was analyzed. Both sheets have an initial thickness of 1 mm and an electrical discharge texture (EDT). While DC04 is commonly used for challenging geometries [7], AA5182 is applied for non-visible car body parts due to its tendency for strain markings [8].

As already mentioned, DLC coatings exhibit a beneficial tribological behavior in dry sheet metal forming [9]. These coatings are mainly characterized by their chemical inertness and high hardness [10]. According to the ternary phase diagram in [11], DLC coatings are distinguished by their graphite (sp^2), diamond (sp^3) and hydrogen content. Previous investigations have shown that in lubricant-free contact conditions, the adhesion tendency between metal surfaces can be successfully reduced by undoped a-C:H coatings [12]. Therefore, this study focuses on the surface modification of this coating type.

2.1 Deposition and properties of a-C:H coatings

The a-C:H coatings were deposited using a hybrid physical vapor deposition (PVD)/ plasma enhanced chemical vapour deposition (PECVD) coating machine (H-O-T, TT-300) with a twofold rotating charging rack. The basic coating system consists of a chromium (Cr) adhesive layer, a tungsten-carbide (WC) interlayer, an a-C:H:W interlayer and the a-C:H functional layer, as shown in Fig. 1. For the Cr adhesive layer and the WC/a-C:H:W interlayers arc evaporation and (reactive) unbalanced magnetron sputtering were used as coating technologies, respectively. The a-C:H coating functional layer was deposited by a pure PECVD process using C_2H_2 as precursor gas. The substrate bias voltage U_{bias} and the deposition temperature were -550 V and 100 °C, respectively. The deposition time for a-C:H layers were kept constant at 8580 s. The C_2H_2 gas flow was 220 sccm and the Ar gas flow was 40 sccm, resulting in a C_2H_2/Ar ratio of 5.5:1.

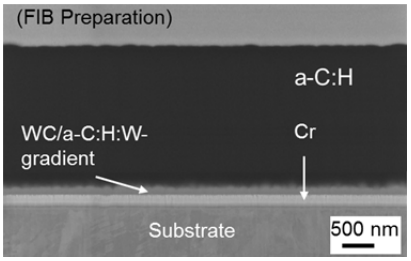

Fig. 1 Setup of the a-C:H coating system using FIB preparation

After deposition, the coating samples were characterized regarding coating thickness and adhesion to substrate using calotte grinding method [13] and Rockwell C adhesion test [14], respectively. Hardness and indentation modulus were measured by micro hardness indentation according to [15]. The a-C:H functional layer was deposited between 80 °C and 100 °C. The mechanical properties of the a-C:H coating system and the substrate are summarized in Table 1.

Table 1 Mechanical properties of coated and uncoated discs

	a-C:H	Substrate
Thickness t of the coating system in µm (n = 5)	2.34 ± 0.07	–
Thickness t of a-C:H functional layer in µm (n = 5)	1.78 ± 0.04	–
Adhesion HF (n = 5)	< HF4	–
Hardness HV 0.001 (n = 12)	1936.8 ± 109.5	1007.0 ± 113.0
Indentation modulus E_{IT} in GPa (n = 12)	502.7 ± 28.9	507.41 ± 48.1

Table 1 shows that the thickness of the total coating system is 2.34 ± 0.07 µm whereby the a-C:H functional layer is 1.78 ± 0.04 µm. All coating samples have an adhesion better than HF4, which represents a sufficient adhesion with small cracks and delamination around the Rockwell indentation according to [14]. The micro hardness and indentation modulus of coating samples are 1936.8 ± 109.5 HV 0.001 and E_{IT} = 502.7 ± 28.9 GPa (n = 12), respectively.

2.2 Surface treatment and characterization of a-C:H coated surfaces

Former studies revealed that the roughness of the tool surface has an essential influence on the tribological conditions especially under dry conditions [16]. Therefore, the aim of this study is to further analyze how the tribological behavior of coated surfaces can be adapted by modifying the topography of the tools. An overview of the investigated surface treatments is given in Table 2.

Table 2 Variants of sequences of mechanical surface treatment steps prior and after coating deposition

Variant	Treatment before deposition	Treatment after coating deposition
(A)	Rough polished	Mechanical
(B)	Smooth polished	Mechanical
(C)	Smooth polished	Laser based

One approach was to change the tool roughness by means of a varying mechanical surface treatment (variant A/B). In a first step, the tool roughness before the coating deposition was varied. All substrate surfaces were polished with a minimum grain size of 9 µm to a roughness of $R_z = 0.9 \pm 0.1$ µm and $R_{pk} = 0.1 \pm 0.01$ µm ($n = 5$), which represents the surface qualities of conventional deep drawing tools without preferential direction. Some of the tool surfaces were additionally polished with a minimum grain size of 3 µm to achieve a smoother topography before coating deposition (variant B). The rough and smooth polished surfaces were afterwards coated according to the process described in 2.1. As the coating process leads to an increase of the surface roughness a post treatment of the coated surfaces was necessary. Therefore, the rough and the smooth polished a-C:H coated surfaces were mechanically post treated for variants A and B. The post treatment was performed manually with 3 µm and 1 µm diamond suspensions each for 15 min. Variant C was post treated by the laser based process which is described in the next section. In order to analyse the influence of the varying surface treatment on the tool roughness a characterization of the tool surfaces was performed prior and after the tribological experiments. The tactile stylus and optical surface measurements of the tool surfaces are conducted with the *Mar Surf GD 120* and the nanofocus *µSurf* microscope, respectively.

2.3 Setup and method for laser based finishing

For ultrashort pulsed laser finishing a mode-locked Nd:YVO_4 laser system (Fuego, Time-Bandwidth Products) with a pulse duration $\tau_P = 10$ ps (FHWM) and wavelength $\lambda = 1064$ nm was used. The laser beam was focused by a telecentric f-Theta lens with a focal length of 160 mm resulting in a beam waist radius ($1/e^2$) $w_0 = 30$ µm. The focused laser beam was deflected by the galvanometer scanner hurryScan 14 II (Scanlab AG). Laser based finishing was performed at room temperature and in normal atmosphere. After laser finishing the laser treated surfaces were cleaned for 3 min in an ultrasonic bath with isopropanol to remove any residues.

2.4 Method for tribological characterization

The tribological behavior of a-C:H coated tool surfaces with varied topographies was analyzed in the flat strip drawing test. This setup models the tribological conditions in the flange area of a deep drawing process and thus enables more process like conditions than tribometer tests with a closed tribological system. The tribological behaviour modelled in the strip drawing test is comparable to the behaviour in the strip bending rotation test [17]. Thus the general findings regarding the tribological relations can be transferred also to the die radius. The friction jaws have a contact area of 55 mm x 100 mm. The strips are 65 mm wide. The basic setup is schematically shown in Fig. 2. The strips are located between an upper and a lower friction jaw and are clamped on one side. The lower friction jaw applies the defined normal force F_N by moving upwards. Then the strips are drawn through the jaws with the drawing force F_D which equals the sum of upper and lower friction forces on both friction jaws F_F. By applying the Coulomb friction law the friction coefficient μ is determined. As evaluation area the measured forces between 100 mm to 170 mm drawing length are considered because here constant normal forces F_N and constant drawing velocities v_{rel} are ensured.

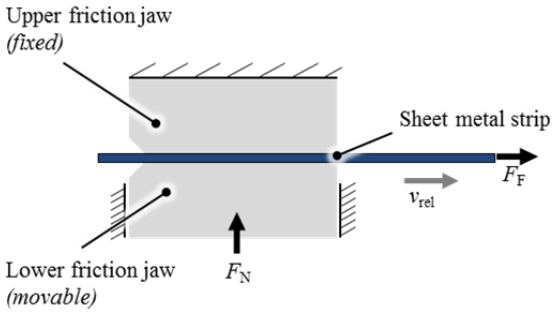

Fig. 2. Experimental setup of flat strip drawing tests (schematically)

Dry strips which were cleaned in an acetone bath were used in all strip drawing tests. The proper removal of anti-corrosive oil and dirt particles was checked using an infrared sensor. A constant drawing velocity v_{rel} of 100 mm/s was applied which is a typical velocity for deep drawing processes. According to characteristic values of the binder pressure, the contact pressure p_N for DC04 was set to 4.5 MPa while for AA5182 a lower pressure of 1.5 MPa was chosen. The lower pressure was choosen due to the lower tensile strength and higher adhesion tendency of AA5182 which leads to a hampered material flow in the flange area. Thus a lower binder pressure is beneficial to improve the material flow.

2.5 Characterization of post treated a-C:H coated surfaces

The micro hardness of a-C:H coatings was determined by Vickers indentation (Fischerscope HM2000, Helmut Fischer GmbH) with an indentation force of 10 mN in 10 s according to DIN EN ISO 14577-1 [15] at 7 points for each modified region. The analyzation of structural properties of the (modified) a-C:H coatings was done by micro Raman spectroscopy (alpha 300RA, WITec). Inelastic scattering of the laser excitation wavelength $\lambda_{Raman} = 532$ nm was recorded to investigate chemical bond configuration. The Raman spectrum was evaluated in the range of 800 to 2700 cm^{-1} where a-C:H coatings

have their characteristic peaks [18]. Undesired modifications of the coating structure were avoided by focusing the applied laser power of 10 mW by a 10x objective on the coating surface [19]. The intensity of the G and D peaks was calculated after decomposition of the recorded spectra by the combination of a linear fit for the background as well as a Breit-Wigner-Fano (BWF) and a Lorentzian model [18].

3 Surface quality and tribological behavior of a-C:H coated tool surfaces

3.1 Ultrashort pulsed laser finishing

Finishing by ultrashort pulsed laser based material removal was investigated as an alternative process to mechanical finishing technologies of a-C:H coatings. In general, laser finishing offers the opportunity of contactless and fast machining due to high-speed beam deflection. Thus, the laser applied as finishing tool is no subject to wear. Therefore, reproducibility of reduced roughness parameters should be increased by automated contactless laser machining compared to mainly manually performed mechanical finishing processes. Particularly, ablation by picosecond laser pulses enables modification of the surface topography with almost no heat input. Therefore, structural and mechanical properties of the carbon-based coatings are expected to remain unaffected by this finishing technology. Each of the laser finished surfaces was characterized by areal roughness parameters within the following investigations. Areal roughness parameters were used to prevent any unwanted influence of existing preferential direction of laser based generated surface topographies on roughness measurements. According to ISO 25178 [20] roughness parameters were optically ascertained by confocal laser scanning microscopy (LSM) with 20x magnification and lateral dimensions of the evaluated region of interest about 540x640 µm (λ_C = 250 µm; λ_S = 2.5 µm).

3.1.1 Material parameters to describe picosecond laser ablation of a-C:H coatings

The selection of appropriate peak fluences to reduce the surface roughness as well as to achieve minimal dimensions of possible heat affected zones requires the knowledge of the material dependent ablation threshold. Furthermore, this threshold fluence F_{th} and the energy penetration depth κ were used to calculate the surface topography and the microscopic shape of the treated region (Fig. 3a) which is generated by the superposition of subsequent crater geometries (Fig. 3b) resulting from the material removal with a Gaussian intensity profile by a single pass. The achieved depth t at position (x,y) is calculated according to eq. (1) which represents an advancement of a published model describing pulsed micromachining of metals [21]:

$$t(x,y) = \sum_{i=1}^{N_x}\sum_{j=1}^{N_y}\left[\kappa(N_{xy})\cdot ln\left(\frac{F(x+i\cdot p_x,y+j\cdot p_y)}{F_{th}(N_{xy})}\right)\right] \quad (1)$$

where $\kappa(N_{xy})$, $F_{th}(N_{xy})$ and N_{xy} describe the pulse number dependent energy penetration depth, the pulse number dependent threshold fluence and the effective pulse number per area. The effective pulse number per area N_{xy} along the beam paths for a single pass of the laser treated region is calculated according to eq. (2) [22]:

$$N_{xy}(w, v_S, f_P, p_y) = \frac{(1.25\cdot w)^2}{p_x\cdot p_y} = \frac{(1.25\cdot w)^2\cdot f_P}{v_S\cdot p_y} \quad (2)$$

where w, v_S, f_P and p_y describe the beam radius, the scanning speed of the laser beam, the pulse repetition rate and the hatch distance applied for subsequent parallel beam paths, respectively. N_x and N_y are the ratios of the two-fold beam radius w and the number of laser pulses which are positioned per $2\cdot w$ depending on p_x and p_y : $N_x = 2\cdot w/p_x$ and $N_y = 2\cdot w/p_y$. The fluence distribution $F(x+i\cdot p_x,y+j\cdot p_y)$ of the Gaussian beam depending on the positions of the laser spot can be calculated according to eq. (3):

$$F(x + i\cdot p_x, y + j\cdot p_y) = F_0 e^{-2\frac{(x+i\cdot p_x)^2+(y+jp_y)^2}{w^2}} \quad (3)$$

where F_0 is the applied peak fluence. The logarithmic dependence of the ablation depth on the applied peak fluence according to eq. (1) is based on the simplified correlation between the optical penetration depth and the exceeded threshold intensity for material ablation under the constraint of no heat conduction by the lattice as it is reasonable for ultrashort laser pulses [23].

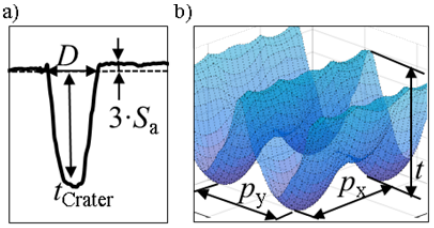

Fig. 3. a) Cross-section of an ablated crater and b) typical ablated topography generated by several laser pulses superpositioned with pitch p_x and hatch p_y

The threshold fluence F_{th} and the energy penetration depth κ were determined by the evaluation of the crater diameter and depth according to the zero-damage-method [24] and logarithmic correlation between depth and peak fluence based on Beer's law [25]. The craters were generated on a-C:H coated samples which were mechanically polished after coating deposition to achieve low roughness $S_a = 0.02 \pm 0.01$ µm and $S_{pk} = 0.06 \pm 0.01$ µm ($n = 5$) to enable automatized detection and evaluation of the crater dimensions with high precision. Both parameters F_{th} and κ were investigated for different pulse numbers N which were used to generate craters at f_P = 1 kHz. The determined pulse-number dependent threshold fluences F_{th} are fitted according to eq. (4) [26] (Fig. 4).

$$F_{th}(N) = F_{th}(1) * N^{S-1} \quad (4)$$

The fit is used to consider the incubation behavior which describes the change of the material properties with material-dependent parameter S [26]. S represents a fit parameter which covers several phenomena affecting material incubation which leads to the pulse number dependence of the threshold fluence. Exemplary phenomena are the change of reflectivity and structural modifications [27] due to the mechanical damage by subsequent laser pulses. The fit function published by Jee et al. is applied because this model shows good coincidence for the relevant low pulse numbers $N_{xy} \leq 30$ [25]. The results of the determined penetration depths reveal no significant pulse number dependence as the determined values fluctuate about $\kappa = 29.5 \pm 3.8$ nm. Therefore, constant penetration depth $\kappa = 29.5$ nm is chosen for the calculation of the structure topography.

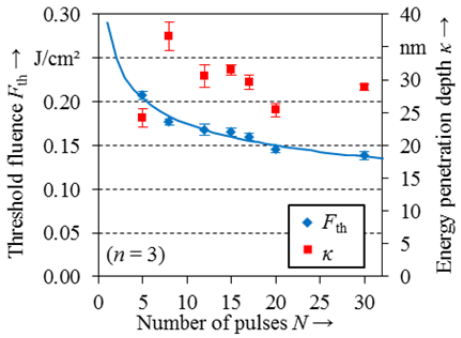

Fig. 4. Pulse number dependent threshold fluence F_{th}, corresponding fitting curve according to Jee et al. and energy penetration depth κ

3.1.2 Influence of Gaussian intensity profile on surface quality

In this chapter, investigations aiming at the tailored energy input and spatial positioning of subsequent laser pulses to minimize the reduced peak height (S_{pk}) of a-C:H coated tools are described. Accordingly, in the order of prioritization low S_{pk}, minimum heat input into the a-C:H coating and minimum reduction of the layer thickness are criteria to assess the laser process and its result. The thickness should be minimally reduced to have a sufficient remaining layer thickness. Low heat input is indicated by low hardness reduction and constant structural properties analyzed by Raman spectrometry. An ablation process with low heat input is characterized by high ablation efficiency which describes the ratio of removed volume divided by the supplied laser pulse energy. Hence, a large part of the laser energy impinging the sample surface causes material ablation.

The samples used for investigations on laser finishing of a-C:H coated tools were smooth polished before the coating process but no mechanical post treatment was applied after layer deposition. The a-C:H coated samples have an arithmetic mean height $S_a = 0.04 \pm 0.01$ µm and reduced peak height $S_{pk} = 0.15 \pm 0.02$ µm ($n = 5$) which are significantly higher compared to additionally mechanically polished surfaces (chapter 2.2). First experimental investigations aim at the selection of an appropriate peak fluence to reduce the surface roughness. For this purpose, the peak fluence was varied at a comparatively low pulse repetition rate $f_P = 1$ kHz to avoid an accumulation of residual heat (Fig. 5a). At peak fluences below 1.0 J/cm² the measured S_{pk} is in the range of the initial roughness of the sample. Additionally, the increased deviation indicates an inhomogeneous material removal. Higher peak fluences lead to significant roughness decrease. The roughness of non-post treated surfaces is mainly reduced due to the removal of asperities by laser ablation. Therefore, the topographies before and after laser finishing differ significantly from each other (Fig. 5c).

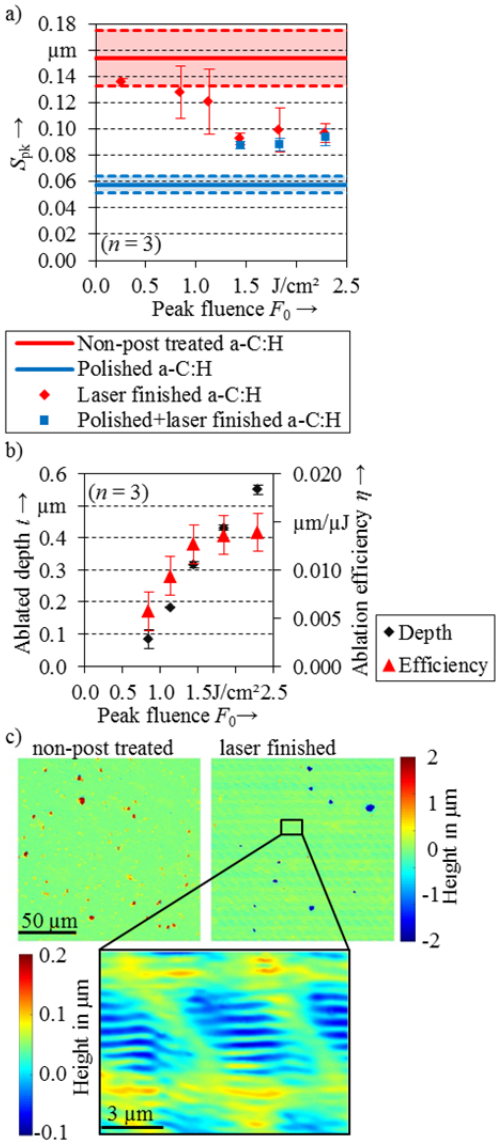

Fig. 5. Influence of peak fluence on a) S_{pk} and b) ablation efficiency; c) topographies of initial non-post treated and laser finished a-C:H surfaces

Acquisitions of the surface topography reveal that the non-post treated coating surface shows more roughness peaks. In contrast to that, these roughness peaks do not appear in regions which were laser finished at higher peak fluences (Fig. 5c). The roughness peaks result from unavoidable droplet deposition during arc evaporation process of the Cr adhesion layer. The removal of droplets is also detectable by a changing reduced valley depth (S_{vk}) due to laser finishing. Initial non-post treated

surfaces reveal $S_{vk} = 0.06 \pm 0.01$ µm ($n = 5$) while the amount and depth of the valleys on areas which were laser finished at 1.5 J/cm² are increased, so that $S_{vk} = 0.14 \pm 0.01$ µm ($n = 3$) is ascertained.

The analysis of the ablated depth reveals the logarithmic increase with increasing fluence (Fig. 5b). Maximum ablation efficiency is achieved at F0 = 1.8 J/cm². At this peak fluence the largest portion of the incident laser pulse energy is removed by ionized and vaporized ablated material and therefore does not remain as residual heat around the generated crater geometry. Any additional increase of the pulse energy would mainly lead to higher distinct heating and a larger heat affected zone. For investigation purposes on the influence of the initial surface roughness of the coating, the peak fluence was varied to process samples which were also mechanically polished after coating deposition. For these samples, S_{pk} values of laser finished samples are higher compared to mechanically post treated samples (Fig. 5a). The measured roughness parameters are similar to the parameters of the non-post treated samples. The minimum fluence dependent S_{pk} seems to be independent from the initial roughness. Thus, the roughness is mainly affected by the topography resulting from laser ablation of superpositioned craters and additional ripples on the processed surfaces (Fig. 5c). Ripple formation is caused by the interference of laser light scattered by the surface roughness and the incident laser beam [28]. On the finished a-C:H surfaces the arising periodic ripples have a width of about 800 nm and a depth of about 150 nm. They are oriented perpendicularly towards the linear polarized laser light. These nanometer scaled structures can limit the achievable minimum S_{pk}. As the minimum S_{pk} and almost maximum ablation efficiency are achieved by using $F_0 = 1.5$ J/cm², this fluence is applied in the following investigations on the tailored spatial separation of the laser pulses to achieve minimum roughness resulting from microscopic topography. For this purpose, hatch distance p_y was varied while scanning speed and pulse repetition rate were kept constant at $v_s = 8$ mm/s and $f_P = 1$ kHz resulting in a pulse-to-pulse pitch of 8 µm. Roughness measurements do not reveal any significant influence on S_{pk} because these parameters are in a range of 0.08 to 0.10 µm for hatch distances 5 µm $\leq p_y \leq$ 11 µm (Fig. 6a). A larger hatch of 14 µm leads to slightly higher S_{pk} and larger standard deviation. Higher fluctuations can indicate locally resisting peaks within regions which are only irradiated with lower fluence, e.g., in the range of flanks of the Gaussian profile. In order to select the proper hatch distance, the surface topographies resulting from ablation by subsequent laser pulses with a Gaussian intensity profile were additionally simulated (Fig. 3b). Based on the fitted and determined parameters $F_{th}(N_{xy})$ and κ described in chapter 3.1.1 the depth of the induced material removal and consequently the arithmetic mean height are calculated. Theoretically calculated depths correspond well with the experimentally evaluated depths (Fig. 6a), so that the applied model is suited to simulate the resulting microscopic topography. However, the calculated average mean heights are about one magnitude lower than the measured ones (Fig. 6b) although the lateral resolutions in the model and the measurements are similar with 0.5 µm and 0.625 µm, respectively. The deviation can be explained by the ripple pattern which occurs at the ground of each superpositioned crater (Fig. 5b). The model does not include the formation mechanisms of ripples and thus, this pattern on the nanometer scale is not illustrated. Nonetheless, the model substantiates the choice of tailored hatch distance, as minimal measured as well as calculated S_a due to minimal roughness on the micrometer scale is achieved by $p_y = 8$ µm.

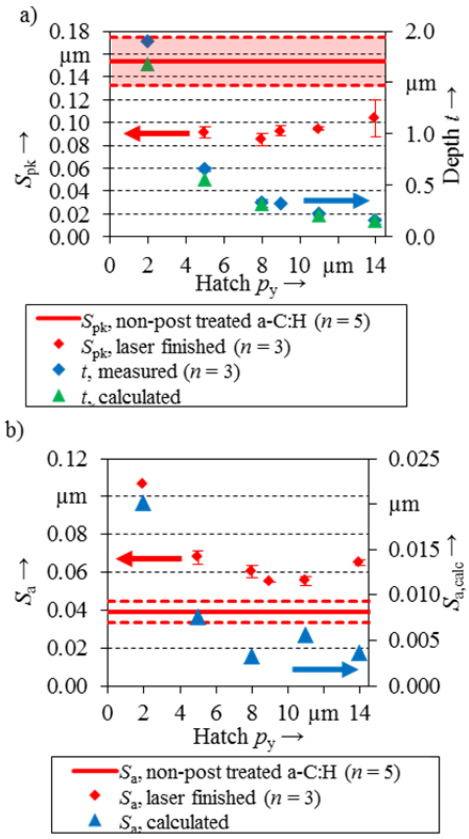

Fig. 6. Influence of hatch distance on a) measured S_{pk} and ablated depth t as well as on b) arithmetic mean height S_a received from experiments and simulations

Based on these results, further investigations on process acceleration to allow fast finishing of tool surfaces are carried out with a hatch $p_y = 8$ µm. For this purpose, the scanning speed is scaled proportionally to the increased pulse repetition rate to keep the pulse pitch p_x constant. These experiments aim at constant roughness as well as structural and mechanical properties. For the examined pulse repetition rates, S_{pk} remains constant within the standard deviation (Fig. 7a). The structural properties of the initial and the laser finished a-C:H coatings are evaluated by the I_D/I_G-ratio derived from Raman spectroscopy according to the methodology described in chapter 2.5. As the I_D/I_G-ratio is drastically higher for laser finished a-C:H coatings than for non-post treated coatings (Fig. 7b), picosecond laser based ablation with $\lambda = 1064$ nm seems to induce formation of heat affected zones which are characterized by an increased degree of sp² hybridization. The

transformation of sp³ in sp² hybridized phases due to laser based ablation and heating is independent from the applied pulse repetition rate because I_D/I_G-ratio remains constant for each laser parameter set. Therefore, accumulation of residual heat after laser ablation seems to have no influence on the structural properties although the time interval between two consecutive laser pulses is reduced up to factor 100. The increase of the degree of sp² hybridization due to laser finishing is also detectable by an hardness decrease of laser treated areas compared to initial a-C:H coatings (Fig. 7c). This hardness drop is also independent of the pulse repetition rate between 1 kHz and 100 kHz.

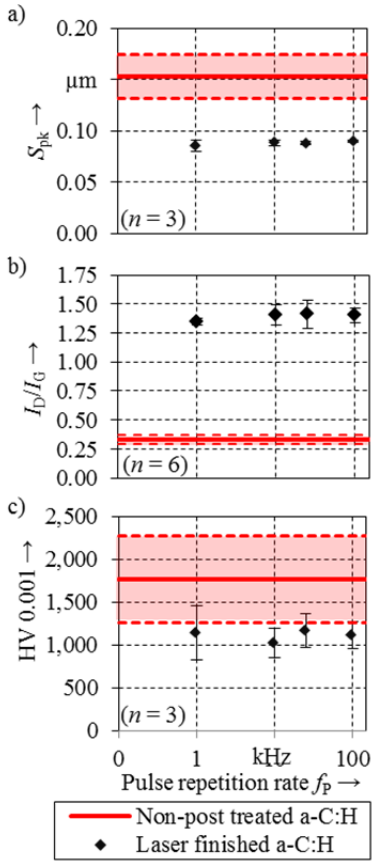

Fig. 7. Dependence of a) S_{pk}, b) I_D/I_G-ratio and c) Vickers hardness on the pulse repetition rate applied for laser finishing

Thus, a high pulse repetition rate can be used for laser finishing enabling fast processing. Exemplary application of the parameter set with $f_P = 100$ kHz for finishing of an a-C:H coated friction jaw would need less than 15 minutes. As the applied pulse energy of 5.1 µJ is much lower than the pulse energy in the range of several hundred µJ of commercially available ultrashort pulsed laser sources, there is further potential to significantly enhance the productivity by process parallelization. For manufacturing purposes of friction jaws for tribological investigations in chapter 3.3 the following parameter set is used: $F_0 = 1.5$ J/cm², $f_P = 25$ k Hz, $v_s = 200$ mm/s, $p_y = 8$ µm. LSM based measurements of regions laser finished with this parameter set reveal $S_{pk} \approx 0.07$ µm ($n = 6$).

3.2 Surface properties of post treated and a-C:H coated tools

The optical measured surface properties after the mechanical and laser based post treatment and before the strip drawing tests are shown in Fig. 8.

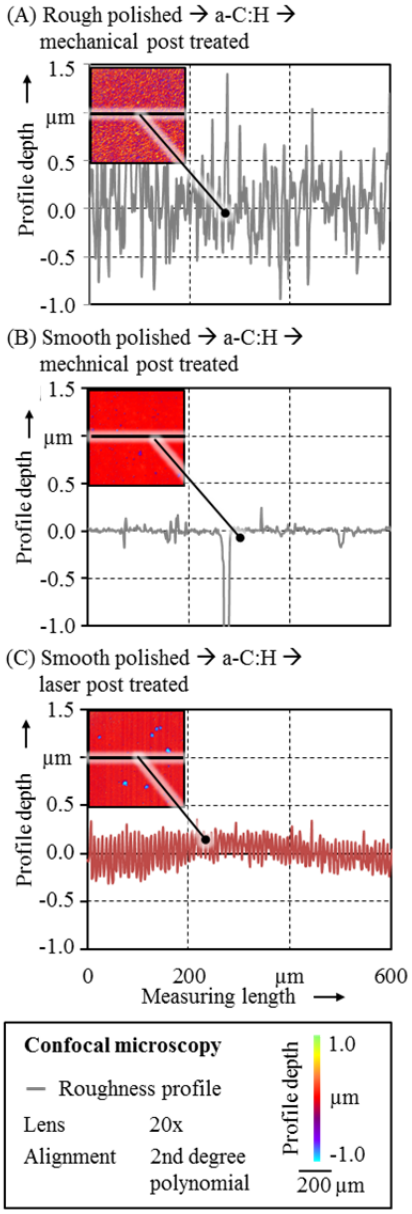

Fig. 8. Surfaces of friction jaws after applied variants of post treatment

Both topographies with mechanical post treatment reveal a surface without preferential direction. A smooth polishing before the coating deposition leads to a surface with few and small roughness asperities after the mechanical post treatment. In contrast, a significantly rougher surface occurs after post treatment of the rough polished substrates. Single roughness peaks achieve heights of over 1 µm whereas the smooth surfaces (variant B) achieve maximum heights of 0.25 µm. The laser based post treatment revealed a preferential direction in form of ripples in drawing direction according to the direction of the laser beam movement.

The height and depth of these ripples which occur due to the laser treatment have an amplitude of 0.25 µm. The height of single roughness asperities is in the same range as for variant B. Additionally some deep valleys result from the coating process which can clearly be seen in the smoother variants B and C. Reason for these pores on the coated surfaces are determinations in the coating chamber or the formation of droplets during arc evaporation of the chromium layer.

3.3 Influences on lubricant-free sliding in strip-drawing tests

The above described methods of mechanical surface treatment and laser based finishing were used to manufacture friction jaws with a-C:H coatings and varying surface roughness. Hence, the influence of the post treatment strategy and the tool roughness on the tribological behavior could be evaluated with the help of strip drawing tests. For the laser based finishing the parameter set which was mentioned in the last section of 3.1.2 was selected to achieve a reduced peak height. The resulting friction coefficients for the different tools surfaces are shown in Fig. 9. In order to describe the tool roughness the reduced peak height of each tool surface is related to the resulting friction. This value is especially important under dry conditions because mainly the roughness asperities of tool and sheet surface are in contact. Thus more or higher asperities have a direct influence on the mechanical interlocking and the resulting resistance towards relative movement.

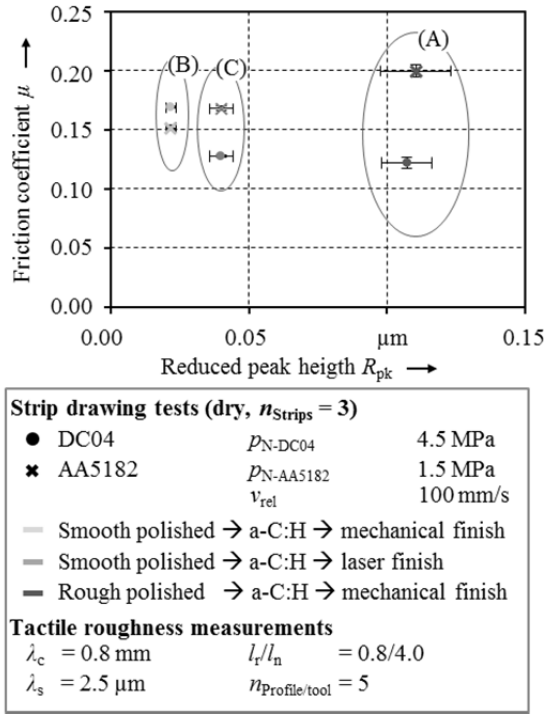

Fig. 9. Influence of tool roughness of a-C:H coated jaws on friction coefficients

Compared to the laser finishing with a reduced peak height of around 0.039 µm a slightly lower roughness is achieved with the mechanical finishing with R_{pk} values around 0.022 µm. A much higher tool roughness with a reduced peak height above 0.10 µm reveals for the friction jaws of variant (A). With smooth polished mechanical finished friction jaws similar friction coefficients between 0.15 and 0.17 are determined for DC04 and AA5182 although a higher contact pressure was applied for DC04. A comparison of the influence of the tool surface treatment on the friction depending on the sheet material is possible even for different levels of contact pressure because the impact of the pressure is low in dry tests [4]. For an increasing tool roughness both sheet materials reveal a different behavior. For DC04 the friction coefficient decreases slightly to a level of 0.13 when a laser based finishing is applied. In contrast, for strips out of AA5182 the friction coefficient increases from 0.15 to 0.17. When the roughness of the friction jaws exceeds 0.1 µm for the R_{pk} value a further increase of friction to 0.2 is measured for AA5182. In contrast, for DC04 the friction coefficient remains at the same level as for the smoother tool surfaces. Thus, there seems to be dependence between the influence of the tool roughness and the sheet material. The different behavior can be explained by the varying surface and mechanical properties between DC04 and AA5182. DC04 has a topography with many plateaus whereas the surface of AA5182 consists of many roughness asperities which are more likely to interact with the asperities of rougher tool surfaces e.g. at the ripples of variant (C). Furthermore, the applied DC04 has a soft zinc coating which smoothens more easily in contact with the tool surfaces. Thus, the risk of interlocking asperities is reduced by a smoothening of the sheet surface. Due to the above mentioned properties of DC04 rougher tools can be applied without risking an increase of friction and wear which can be seen in Fig. 7 for variant (A). In order to ensure that the coated tools lead to a generally beneficial tribological behavior independent from the sheet surface a topography with lower R_{pk} values should be preferred.

The tool surfaces were characterized after the strip drawing tests in contact to AA5182. On a macroscopic scale no distinctive wear was visible. Therefore, a microscopic analysis was performed. With the normally used lens with 20x magnification no distinct wear marks could be detected. However, a small amount of adhesive material was identified using 50x magnification. In a previous study [29] such metallic adhesions were investigated by EDX analysis. It was observed that the adhesion on the a-C:H coating surface against AA5182 consists mainly of oxygen, magnesium and aluminium and against DC04 mainly of oxygen and zinc [29]. Representative tool topographies for the different surface treatments are compared in Fig. 10 regarding the profile depth and their reflectivity. For variant (A) a locally increased profile depth was measured in the range of 1 µm. For variant (B) and (C) it was not possible to clearly identify wear in the topography pictures. Looking at the reflection pictures shown in the second row in Fig. 10, the brighter regions indicate metallic adhesion which has higher reflectivity than the coating itself. Adhesive wear occurred also for variant (C) especially on pores resulting from the coating deposition process.

For the smoother tool surfaces which were achieved with variant (B) no adhesion occurred. Overall, the highest amount of adhesive wear was measured for the rough polished surface of variant (A). This is accordance with the strip drawing tests where these friction jaws revealed the highest friction coefficient for AA5182.

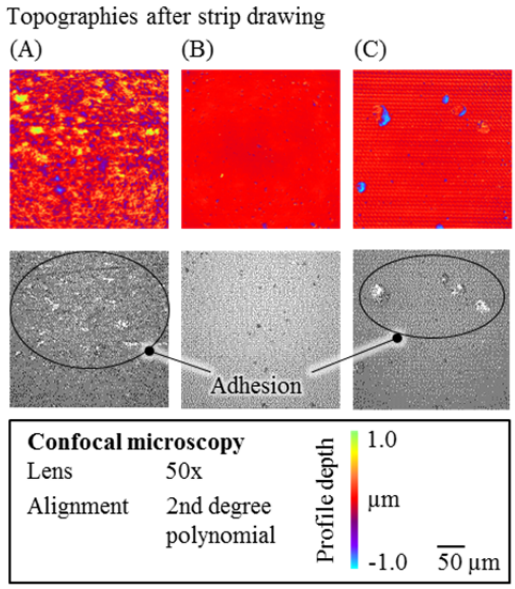

Fig. 10. Topographies and reflectivity of friction jaw surfaces after strip drawing tests in contact to AA5182

Besides the roughness the Raman spectra and hardness of the tools was measured before the strip drawing. The results are shown in Fig. 11 a) and b). An increasing ratio of I_D/I_G indicates a growing amount of sp^2 (graphite-like) content which means that the amount of sp^3 hybridization (diamond-like) phases is reduced. The mechanical finished surfaces reveal nearly the same I_D/I_G ratio as the not finished friction jaws before the laser based treatment. After the laser based finishing process the ratio increased from around 0.3 to 1.4. The changed hybridization is the reason for the changes of the coating hardness which is depicted in Fig. 11 b). For laser finished friction jaws the hardness was measured before and after the laser based finishing. The rough and the smooth polished a-C:H coated surfaces revealed a hardness between 1560 and 1860 HV0.001 after the mechanical post treatment. The smooth polished variant (B) revealed a lower standard deviation due to the improved surface quality which influences the results of hardness measurements. For the friction jaws of variant (C) a hardness of 1725 HV0.001 was measured before the laser based finishing. After the post treatment, the hardness decreased to a significantly lower level of around 1000 HV0.001 due to the heat impact of the laser treatment. It is known from former studies that with decreasing hardness the friction coefficient increases for hydrogenous carbon based coatings deposited in PVD processes [30]. Thus, besides the slightly higher R_{pk} values the lower hardness might be a further reason for the increase of friction from 0.151 to 0.169 for AA5182. This hardness drop caused by laser treatment should be reduced by appropriate measures concerning ultrashort pulsed laser finishing in future investigations.

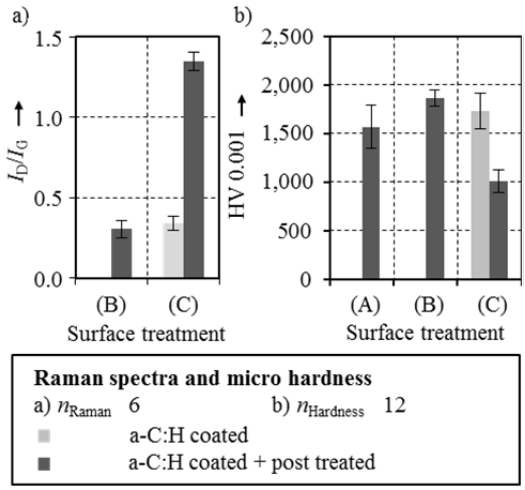

Fig. 11. a) Raman spectra and b) Vickers hardness of tool surfaces in dependence of surface treatment

4 Conclusion and outlook

In this study the tribological behavior of a-C:H coated tool surfaces was analyzed under dry conditions with the help of strip drawing tests. Especially, the influence of a varying roughness of the coated surfaces was investigated. Different roughness values were achieved by varying the pre and post treatment processes. In addition to commonly used mechanical surface treatments a laser based finishing process was investigated. The coating process leads to an increased amount and height of roughness asperities. Reasons for the increasing roughness are droplets occurring during the arc evaporation process of the chromium adhesive layer and possible contaminations within in the coating chamber. The laser based finishing enables a reduction of the S_{pk} values by removing single roughness asperities. In order to identify the necessary process parameters for the laser treatment an analytical model of the material removal was applied. Supported by the model a suitable spatial separation of the pulses was determined to achieve a minimum roughness. However, the model is not able to predict specific roughness values but trends for the roughness development depending on the spatial separation. The final roughness values are not only influenced by removal of asperities but by the formation of ripples. These ripples are caused by interferences of the linear polarized laser beam on the surface and cannot be avoided with the applied system technology. Besides the formation of ripples which influence the tool topography, the hardness of the a-C:H coatings is reduced due to the heat impact of the laser pulses. The heat input leads to a structural change of the coating composition by increasing the sp^2 content. Thus, the coating consists of more graphite and less diamond phases which explains the reduction of the hardness. The tribological behavior of laser treated a-C:H coatings in direct contact with DC04 and AA5182 was compared to mechanical treated friction jaws. Smooth polished surfaces revealed only slightly higher S_{pk} values for laser based finishing compared to mechanical finishing after coating deposition. Rough polished substrates revealed

much higher S_{pk} values after the mechanical finishing. For DC04 an increasing tool roughness did not lead to higher friction coefficients. In contrast, for AA5182 the friction coefficient increases with increasing S_{pk} values. Additionally, the adhesion tendency increases which results in adhering of the sheet material on the coated surfaces at a microscopic scale. Reason for the 13 % higher friction coefficient for laser finished compared to mechanical finished tools in contact with AA5182 might be the increased sp^2 content evoking a lower hardness in combination with the slightly higher S_{pk} values. The tribological investigations revealed that for dry deep drawing of zinc coated DC04 a broader range of S_{pk} values leads to acceptable tribological conditions whereas for AA5182 a smooth tool surface has to be ensured to utilize the full potential of a-C:H coatings. In future investigations additional developments regarding the coating deposition process and the surface finishing will be analyzed to further improve the tribological behavior of a-C:H coatings under dry conditions. The influence of a structural multilayer design on coating properties and tribological behavior will be analyzed. The wear resistance will be increased by targeted adjustment of the hardness to indentation modulus ratio through variation of coating parameters such as bias voltage and gas flow. Regarding the laser based finishing further tests with a homogenous intensity profile [31] and femtosecond pulse duration will be performed to reduce the heat-affected zone and restrict the hardness reduction and structural changes. Future investigations have to show to which degree a hardness reduction and structural changes can be limited [17].

The authors thank the German Research Foundation (DFG) for supporting the presented investigations by funding the priority program SPP 1676 project ME 2043/50-1, SCHM 2115/49-1 and TR 1043/5-1 with the project title “Lubricant free forming with tailored tribological conditions”.

References

1. F. Vollertsen, F. Schmidt, IJPEM-GT, **1**, 1 (2014)
2. A. Ghiotti, S. Bruschi, Wear, **271**, 9–10 (2011)
3. V. Weihnacht, A. Brückner, S. Bräunling, VIP, **20**, 3 (2008)
4. M. Merklein, M. Schmidt, S. Tremmel, K. Andreas, T. Häfner, R. Zhao, J. Steiner, OAJ FMT, **3**, pp. 42–56 (2015)
5. J. Vetter, Surf. Coat. Technol., **257**, pp. 213–240, (2014)
6. J. Steiner, K. Andreas, M. Merklein, ASHMET (Eds.) Proc. Int. Deep Drawing Research Group Conf., pp. 679–688 (2016)
7. A. Birkert, S. Haage, M. Staub, *Umformtechnische Herstellung komplexer Karosserieteile*, Springer (2013)
8. E. Romhanji, M. Popović, D. Glišić, M. Stefanović, M. Milovanović, Metallurgija, **10**, pp. 205–216 (2004)
9. J. Steiner, K. Andreas, M. Merklein, IOP Conf. Ser. Mater. Sci. Eng., **159**, 1 (2016)
10. Association of German Engineers (VDI), *VDI Guideline 2840*, Beuth (2012)
11. Y. Lifshitz, G. D. Lempert, E. Grossman, Phys. Rev. Lett., **72**, 17 (1994)
12. J. C. Sánchez-López, A. Fernández, Tribology of Diamond-Like Carbon Films, C. Donnet, A. Erdemir (Eds.), Springer (2008)
13. German Institute for Standardization (DIN): DIN EN ISO 26423. Beuth (2016)
14. Association of German Engineers (VDI), *VDI Guideline 3198*, Beuth (1992)
15. German Institute for Standardization (DIN), DIN EN ISO 14577, Beuth (2003)
16. B. Podgornik, J. Jerina, Surf. Coatings Technol., **206**, 11–12, pp. 2792–2800 (2012)
17. J. Tenner, T, Häfner, B. Rothammer, K. Krachenfels, R. Zhao, M. Schmidt, S. Tremmel, M. Merklein, OAJ FMT, **4**, pp. 35–46 (2018)
18. A.C. Ferrari, J. Robertson, Phil. Trans. R. Soc. Lond. A, **362**, pp. 2477–2512 (2004)
19. S. Prawer, K.W. Nugent, Y. Lifshitz, G.D. Lempert, E. Grossman, J. Kulik, I. Avigal, R. Kalish, Diamond Relat. Mater., **5**, pp. 433–438 (1996)
20. German Institute for Standardization (DIN): DIN EN ISO 25178, Beuth (2011)
21. D.A. del Cerro, Dissertation, Mechanical Automation, University of Twente, Enschede (2014)
22. L. M. Machado, R. E. Samad, W. de Rossi, and N. D. Vieira Junior, Opt. Expr., **20**, pp.4114–4123 (2012)
23. S. Nolte, C. Momma, A. Jacobs, A. Tünnermann, B.N. Chichkov, B. Welleghausen, N. Welling, J. Opt. Soc. Am. *B,* **14**, 10, pp. 2716–2722 (1997)
24. J.M. Liu, Opt. Lett., **7**, pp. 196–198 (1982)
25. T. Häfner, J. Heberle, M. Dobler, M. Schmidt, J. Laser Appl., **28**, pp. 0226051–0226056 (2016)
26. Y. Jee, M.F. Becker, R.M. Walser, J. Opt. Soc. Am. B, **5**, pp. 648–659 (1988)
27. A. Naghilou, O. Armbruster, W. Kautek, Appl. Surf. Sci., 418, pp. 487–490 (2017)
28. J. Bonse, S. Höhm, S.V. Kirner, A. Rosenfeld, J. Krüger, IEEE J. Sel. Top. Quantum Electron., **23**, pp. 1–15 (2017)
29. R. Zhao, S. Tremmel, TEWISS (Eds.) Proceedings of THE «A» Coatings 2016, **IFW 3**, pp. 193–200 (2016)
30. C. Zhang, M. Fujii, J. Surf. Eng. Mater. Tech., **5**, pp. 110–123 (2015)
31. T. Häfner, J. Strauß, C. Roider, J. Heberle, M. Schmidt, Appl. Phys. A, 124:111 (2018)